

The Cosmic Large-Scale Structure in X-rays (CLASSIX) Cluster Survey I: Probing galaxy cluster magnetic fields with line of sight rotation measures

Hans Böhringer¹, Gayoung Chon¹ and Philipp P. Kronberg²

¹ Max-Planck-Institut für extraterrestrische Physik, D-85748 Garching, Germany.

² Department of Physics, University of Toronto, 60 St George Street, Toronto, ON M5S 1A7, Canada

Submitted 08/05/16

ABSTRACT

To search for a signature of an intracluster magnetic field, we compare measurements of Faraday rotation of polarised extragalactic radio sources in the line of sight of galaxy clusters with those outside. To this end, we correlated a catalogue of 1383 rotation measures of extragalactic polarised radio sources with galaxy clusters from the CLASSIX survey (combining REFLEX II and NORAS II) detected by their X-ray emission in the ROSAT All-Sky Survey. The survey covers 8.25 ster of the sky at $|b_{ll}| \geq 20^\circ$. We compared the rotation measures in the line of sight of clusters within their projected radii of r_{500} with those outside and found a significant excess of the dispersion of the rotation measures in the cluster regions. Since the observed rotation measure is the result of Faraday rotation in several presumably uncorrelated magnetised cells of the intracluster medium, the observations correspond to quantities averaged over several magnetic field directions and strengths. Therefore the interesting quantity is the dispersion or standard deviation of the rotation measure for an ensemble of clusters. In the analysis of the observations we found a standard deviation of the rotation measure inside r_{500} of about $120 (\pm 21) \text{ rad m}^{-2}$. This compares to about $56 (\pm 8) \text{ rad m}^{-2}$ outside. Correcting for the effect of the Galaxy with the mean rotation measure in a region of 10 deg radius in the outskirts of the clusters does not change the outcome quoted above. We show that the most X-ray luminous and thus most massive clusters contribute most to the observed excess rotation measure. Modelling the electron density distribution in the intracluster medium with a self-similar model based on the REXCESS Survey, we found that the dispersion of the rotation measure increases with the column density, and we deduce a magnetic field value of about $2 - 6 (l/10 \text{ kpc})^{-1/2} \mu\text{G}$ assuming a constant magnetic field strength, where l is the size of the coherently magnetised intracluster medium cells. This magnetic field energy density amounts to a few percent of the average thermal energy density in clusters. On the other hand, when we allowed the magnetic field to vary such that the magnetic energy density is a constant fraction of the thermal energy density, we deduced a slightly lower value for this fraction of $3 - 10 (l/10 \text{ kpc})^{-1/2}$ per mille. Compared to the situation in the Milky Way, where the ratio of the magnetic to thermal energy density is about unity, this ratio is much lower in galaxy clusters. The reason for this is most probably the different generation mechanism for the magnetic field, which is mostly powered by supernovae in the Galaxy and by turbulence from cluster mergers in galaxy clusters. The latter process sets a natural upper limit on the growth of the magnetic field.

Key words. magnetic fields, galaxies: clusters, galaxies: clusters: intracluster medium, X-rays: galaxies: clusters

1. Introduction

In the past decades we have gained much insight into the structure and physics of galaxy clusters from observations of their hot intracluster medium (ICM), which enabled us among other things to measure their masses, characterise their dynamical state, and use them to study the large-scale structure of the Universe (e.g. Voit 2005, Böhringer & Werner 2010, Kravtsov & Borgani 2012, Chon et al. 2012). In most of these studies the ICM was treated as a thermal plasma, and magnetic fields were ignored. On the other hand, we know that magnetic fields are present, mostly through the observation of synchrotron radiation and Faraday rotation of polarised radio signals from background radio sources. The radio synchrotron emission comes from cosmic-ray electrons in the magnetic field of the ICM observed in radio halos and radio relics in clusters (e.g. Kim, et al. 1990, Feretti et al. 2012). The Faraday rotation measure (RM) is imprinted on the signal of polarised radio sources seen in the background in the line of sight of galaxy clusters (e.g. Kim,

Tribble & Kronberg 1991, Feretti et al. 1995, Clarke et al. 2001). Thus a magnetic field seems to be a ubiquitous component of the ICM (e.g. Carilli & Taylor 2002), and for many physical processes its presence needs to be taken into account. In this paper we use the statistics of RMs in the lines of sight through galaxy clusters to infer properties of the cluster magnetic fields.

Polarised electromagnetic radiation traversing a magnetised plasma is subject to Faraday rotation, with a RM given by

$$RM = 811.9 \left(\frac{n_e}{1 \text{ cm}^{-3}} \right) \left(\frac{B_{\parallel}}{1 \mu\text{G}} \right) \left(\frac{L}{1 \text{ kpc}} \right) \text{ rad m}^{-2} \quad (1)$$

For an ICM with typical electron densities of 10^{-3} cm^{-3} , a size of about one Mpc, magnetic fields of a few μG , and a magnetic field aligned with the line of sight, we would expect RMs with values of about 1000 rad m^{-2} . Since the magnetic field is most probably tangled, the effect partly averages out, and for an ordering scale of the magnetic field of about 10 kpc, we expect an RM dispersion at least an order of magnitude smaller than this value. Owing to the frequency dependence of the effect, the

Send offprint requests to: H. Böhringer, hxb@mpe.mpg.de

rotation of the polarisation angle can be determined when the polarisation at more than one frequency is measured. For expected RM values of about 100 rad m^{-2} , the rotation of the polarisation vector at a wavelength of 21 cm, for instance, is 4.42 rad. Measurements at several frequencies are therefore required to derive the RM unambiguously. Observed RM signals in the line of sight of clusters also show, in addition to the effect of the ICM, the imprint of the galactic magnetic field and interstellar medium and possibly a source-intrinsic RM. Typical values for the galactic RM are about 50 rad m^{-2} (Simard-Normandin & Kronberg 1980, Simard-Normandin, Kronberg & Button 1981). This means that there is a high possibility to observe the imprint of the ICM RM with a statistical sample of RMs in galaxy cluster sight-lines.

The first attempt of such a study was conducted by Lawler & Dennison (1982). They found a signature of excess RMs in clusters with about 80% confidence for 12 sight-lines with impact parameters of $< 1/3$ Abell radius and 12 sight-lines at $1/3 - 1$ Abell radii. In their analysis the authors concluded that the typical magnetic field strength is about $0.07 N^{1/2} \mu\text{G}$ with an upper limit of $0.2 \mu\text{G}$, where N is the number of ICM cells with a coherent magnetic field. Kim, Tribble & Kronberg (1991), Feretti et al. (1995), and subsequently others studied the magnetic field in the Coma cluster with RMs along several sight-lines and partly also with RMs of extended radio sources, concluding a magnetic field strength of $< \sim 7 \mu\text{G}$ and an ordering scale of 1 - 10 kpc. Clarke et al. (2001) studied the statistical effect of cluster ICM for 27 sight-lines through X-ray luminous galaxy clusters, and found a clear signal. The galaxy clusters in their sample all had good enough X-ray observations to allow an individual modelling of the properties of the cluster ICM to determine the electron column density in the line of sight. From comparison of the RMs detected in the cluster sight-lines with those measured outside and an analysis of the electron column densities, they deduced an average magnetic field strength of $< |B| > = 5 - 10 (l/10\text{kpc})^{1/2} h_{75}^{1/2} \mu\text{G}$. Since then, several detailed studies of RMs for multiple sight-lines through individual clusters have also been conducted (e.g. Feretti et al. 1999, Murgia et al. 2004, Feretti et al. 2012). A search for magnetic fields on even larger scales has been conducted by Xu et al. (2006), who found a signal of enhanced RM in the Hercules and Perseus-Pisces supercluster implying a magnetic field of $\sim 10^{-7} \text{ G}$ with an upper limit of $\sim 3 \times 10^{-7} \text{ G}$. Kronberg et al. (2007) also found faint radio emission on scales of several degrees (up to 4 Mpc) close to the Coma cluster in the Great Wall region, implying magnetic fields of about $2 - 4 \times 10^{-7} \text{ G}$.

Meanwhile, the number of extragalactic RMs has increased since the study of Clarke et al. (2001), and our catalogue of X-ray detected galaxy clusters with well-understood properties is also much larger, therefore we now revisit the statistical detection of ICM RMs. With the better statistics we can study the correlation of the observed RM with cluster properties in more detail and produce more quantitative results. In total, we now have RMs from 92 sight-lines through clusters, which increases the statistics by about a factor of four.

To determine all distance-dependent parameters, we use a flat ΛCDM cosmology with $H_0 = 70 \text{ km s}^{-1} \text{ Mpc}^{-1}$ and $\Omega_m = 0.3$. All X-ray luminosities are quoted in the 0.1 - 2.4 keV band.

2. Observational data

2.1. X-ray galaxy cluster sample

The galaxy cluster sample CLASSIX that we used here combines for the first time the northern and southern clusters that are identified by their X-ray emission in the ROSAT All-Sky X-ray Survey (Trümper 1993, Voges et al. 1999). The southern sample, REFLEX II (Böhringer et al. 2004, 2013, Chon & Böhringer 2012), covers the southern sky below declination $+2.5^\circ$ and at Galactic latitude $|b_{ll}| \geq 20^\circ$. The survey region, source detection, galaxy cluster sample definition and compilation, construction of the survey selection function, and tests of the completeness of the survey are described in Böhringer et al. (2013). Known galaxy clusters in the region of the Magellanic Clouds, excised in REFLEX II, are included here. The northern sample, NORAS II (Böhringer et al., 2000, Böhringer et al., in preparation), has been constructed in the same way as REFLEX II. The two samples can thus be combined (taking into account the overlap region at declination 0 to $+2.5^\circ$) and described with a common selection function. In total, the catalogue contains 1722 X-ray luminous galaxy clusters.

In summary, the overall survey area is ~ 8.25 ster. The nominal flux-limit down to which galaxy clusters have been identified in the RASS in this region is $1.8 \times 10^{-12} \text{ erg s}^{-1} \text{ cm}^{-2}$ in the 0.1 - 2.4 keV energy band. The nominal flux limit imposed on the survey was calculated from the detected photon count rate for a cluster X-ray spectrum characterised by a temperature of 5 keV, a metallicity of 0.3 solar, a redshift of zero, and an interstellar absorption column density derived from the 21cm sky survey described by Dickey and Lockman (1990). This count rate is analogous to an observed object magnitude corrected for Galactic extinction in the optical.

Spectroscopic redshifts have been obtained for all the clusters, except for 25 missing redshifts in NORAS II, which are excluded here. Based on these redshifts, proper fluxes and X-ray luminosities were calculated iteratively, by using the proper K-correction for the given redshift and assuming an intracluster temperature according to our X-ray luminosity - temperature relation. This relation was determined with the REXCESS cluster survey (Böhringer et al. 2007, Pratt et al. 2009), a representative subsample of the survey clusters.

The most important cluster characterisations are the cluster mass and the fiducial cluster radius. We use r_{500} here for the cluster outer radius, which is defined as the radius inside which the mean mass density of a cluster is 500 times the critical density of the Universe. r_{500} and M_{500} (the mass inside r_{500}) are determined from the relation of the X-ray luminosity and cluster mass as described in Böhringer et al. (2013), with the following luminosity mass relation:

$$M_{500} = 2.48 L_{X,500}^{0.62} E(z)^{-1}, \quad (2)$$

where $E(z)^2 = \Omega_m(1+z)^3 \Omega_\Lambda$.

X-ray emission is observed in most clusters in the ROSAT Survey and in follow-up XMM Newton observations up to a radius close to r_{500} . Thus the characterisation of the cluster ICM is quite reliable out to this radius. The mean typical X-ray luminosity of the cluster sample is $2.3 \times 10^{44} \text{ erg s}^{-1}$ and the mean cluster mass is about $3 \times 10^{14} M_\odot$.

2.2. Sample of rotation measures

To probe the Faraday RMs imprinted by clusters on the line of sight to polarised radio sources, we have drawn from the sam-

ple of Faraday rotation measures shown in Fig. 1 of Kronberg & Newton-McGee (2011). Selecting only measurements at locations with $|b_{II}| \geq 20^\circ$ and removing all known redshifts below $z = 0.05$, which is intended to exclude Galactic sources, leaves 1383 RMs in the sample. Radio sources with double lobes with separate RM determinations are treated as separate sources. Because of the more complex Galactic foreground structure we decided not to extend our survey into the Galactic band $|b_{II}| < 20^\circ$.

We also considered using the RM dataset of Taylor et al. (2009). Apart from the fact that the RM were obtained from only two frequencies, which can lead to ambiguities for high values of RM, we only found two RM sightlines overlapping with clusters for this sample.

Radio wavelengths used in the RM determinations ranged from $\lambda \sim 2$ cm to ~ 31 cm, but this varied from source to source depending on the radio telescopes and available wavelengths. They are an expanded and updated version of the 555 RM sample of Simard-Normandin et al. (1981) and were derived from polarisation measurements at many wavelengths, using methods described in detail by Simard-Normandin et al. (1981). The large available baseline in λ^2 gives an unprecedented average precision in the RM determinations (usually $< \pm 2$ rad m^{-2}) (see Pshirkov et al. 2011).

3. Data analysis

To search for an imprint of RM that is due to clusters of galaxies, we sorted the polarised radio sources with RMs by their distance to the nearest cluster in the sky. As a fiducial radius for the edge of the galaxy clusters we took r_{500} . The value of r_{500} was calculated using the cluster mass obtained from the empirical relation of X-ray luminosity and cluster mass given above, following Böhringer et al. (2013):

$$r_{500} = 0.957 L_{X,500}^{0.207} E(z)^{-1}. \quad (3)$$

Outside of r_{500} in the outskirts of clusters, the column density of the ICM is too low to expect a significant excess RM. The integrated cross section of all clusters in the sample in terms of sky area amounts to 203.8 deg² (0.062 ster, 0.75% of the entire survey area). In total, we found 92 radio sources with known RMs inside the projected cluster locations. Comparison of the radio source and cluster redshifts shows that most of the polarised radio sources are radio galaxies in the clusters. Only 10 are background sources with known redshifts, and for 26 polarised radio sources the redshifts are unknown. We assume that for the radio galaxies in clusters the ray path intersects on average about half of the ICM column density. Thus we can include them as probes for the ICM magnetic field.

Figure 1 shows the observed RMs as a function of cluster-centric distance scaled to r_{500} . We note an obvious enhancement of the scatter of RMs inside r_{500} compared to polarised radio sources at larger distances from the cluster centres. The plot also shows that even though most of these radio sources are hosted in the cluster, the majority are not the central dominant cluster galaxies, which might be located in cooling cores with enhanced magnetic fields, producing particularly high RMs. Calculating the standard deviation of the RM (in the following referred to as the scatter) inside $0.5r_{500}$, r_{500} , and at $0.5r_{500} < r < r_{500}$ and $r_{500} < r < 10r_{500}$, we found the following values of the scatter for the RMs: 123 ± 21 , 120 ± 21 , 144 ± 43 , and 57 ± 6 rad m^{-2} , respectively. These striking results are also summarised in Table 1. The uncertainty of the scatter was determined from 1000

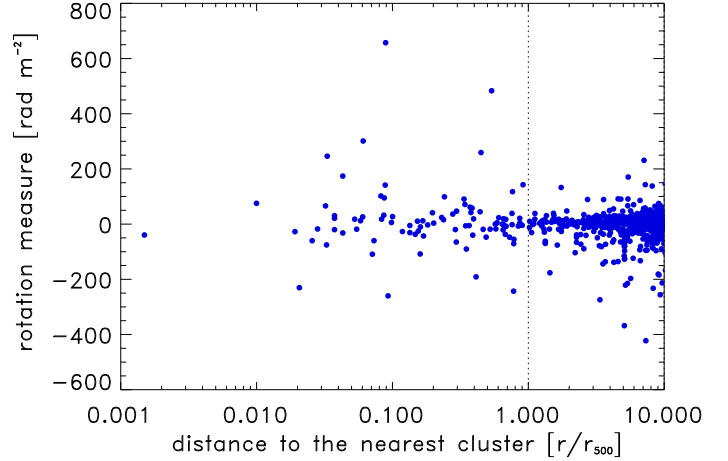


Fig. 1. Rotation measure as a function of cluster-centric distance scaled to the fiducial cluster radius, r_{500} . The vertical dashed line shows a cluster radius of r_{500} .

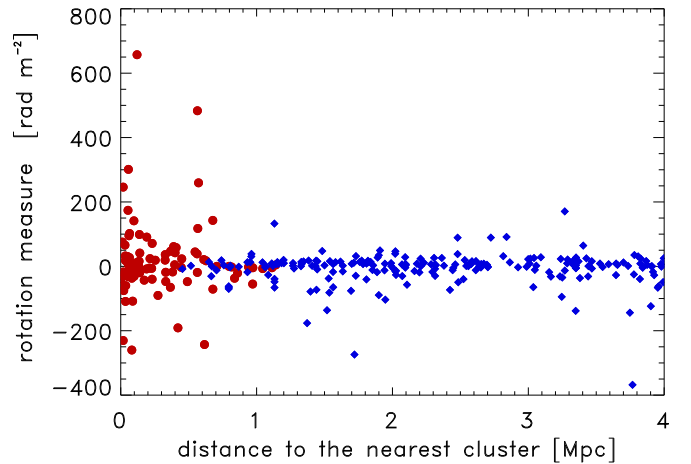


Fig. 2. Rotation measures as a function of cluster-centric distance in physical units (Mpc). The rotation measures inside r_{500} are marked by red circles and those outside by blue diamonds.

bootstrap simulations. One particularly high RM inside r_{500} has a value of 657.3 rad m^{-2} . It is located inside a very massive cluster, Abell 1763, with an X-ray luminosity of 9.2×10^{44} erg s^{-1} corresponding to a mass of $8.3 \times 10^{14} M_\odot$. The radio source itself is a double-lobed wide-angle tail radio galaxy 4C +41.26 in the central region of the cluster (Owen & Ledlow 1997). While there is a chance that the high RM originates locally from the radio source, the fact that it is correlated with a rare high-mass cluster suggests a high probability that the RM is associated with the cluster. Removing this source from the calculations by imposing an RM cut $|RM| < 500$ rad m^{-2} , we obtain the following values for the scatter: 94 ± 13 , 100 ± 15 , 114 ± 43 , and 57 ± 6 rad m^{-2} , respectively. The signal for the clusters has decreased, but is still significantly stronger inside the clusters compared to outside.

Figure 2 also shows the distribution of the RMs as a function of physical radius in units of Mpc for a better comparison with our earlier study reported in Clarke et al (2001). Using physical radii, the signal is also very clear, and the scatter is 115 ± 27 , 111 ± 21 , 68 ± 10 rad m^{-2} for impact parameters < 0.5 Mpc, < 1 Mpc, and outside 1 Mpc, respectively.

Table 1. Standard deviation of the observed rotation measure in different regions in and around the line of sight of galaxy clusters. The different analyses are explained in the notes below. N_e refers to the electron column density in the line of sight.

	$< 0.5r_{500}$	$0.5 - 1r_{500}$	$< r_{500}$	$1 - 10r_{500}$
A	123 ± 21	114 ± 43	120 ± 21	57 ± 6
B	94 ± 13	114 ± 43	100 ± 15	57 ± 6
C	124 ± 21	112 ± 43	120 ± 21	52 ± 6
	$< 0.5\text{Mpc}$	$0.5 - 1\text{Mpc}$	$< 1\text{Mpc}$	$> 1\text{Mpc}$
D	115 ± 27	107 ± 33	111 ± 21	68 ± 10
N_e	$< 6.5 \cdot 10^{20}$	$6.5 - 15.2 \cdot 10^{20}$	$> 6.5 \cdot 10^{20}$	
E	58.6 ± 10.5	122.2 ± 35.6	157.0 ± 40.3	

Notes: **A** RMs uncorrected for the galactic contribution, **B** same as **A** without RMs $|RM| > 500$, **C** with RMs corrected for Galactic contribution, **D** region defined in physical radii, **E** RMs as a function of electron column density given in units of cm^{-2} . The caption for the last line gives the range of electron column densities for the bin. The bin boundaries have been chosen such that each bin has a similar number of RMs.

The clusters in our sample cover a wide mass range from 0.02 to $19.1 \times 10^{14} M_{\odot}$. Smaller clusters will have a lower electron column density of the ICM in the line of sight for a given radius scaled by r_{500} . This indicates that most of the signal comes from the most massive clusters. To test this, we separated the cluster sample into two halves split by the median X-ray luminosity of $0.41 \times 10^{44} \text{ erg s}^{-1}$, which corresponds to a mass of about $1.4 \times 10^{14} M_{\odot}$. Above this median L_X , the scatter of the RM is $158 \pm 34 \text{ rad m}^{-2}$, while for the other half of the sample with lower X-ray luminosity the scatter in the RM is $62 \pm 11 \text{ rad m}^{-2}$. Thus we see a clear sign of the effect, confirming that the observed excess scatter in the RM in the lines of sight of galaxy clusters is due to the cluster ICM. We also checked the redshift distribution of the clusters contributing to the observed excess RM. We find that while the median redshift of the ROSAT cluster sample is about $z = 0.1$, only nine clusters above this redshift have an observed RM. This is probably due to the decreasing apparent size of the clusters with increasing redshift. The 92 RMs found are projected onto 65 clusters. In most clusters only one sight-line with known RM is found. A notable exception is the nearby Coma cluster at a distance of $\sim 100 \text{ Mpc}$, where 12 RMs are in our catalogue and more are known (Kronberg 2016).

4. Results and discussion

Part of the observed RM in the line of sight of clusters comes from the effect of the foreground interstellar medium in our Galaxy. We aimed to correct for this foreground effect by removing the average RM signal in the surroundings of the clusters. To demonstrate the usefulness of such a correction, we studied the distribution of the RMs in the outskirts of clusters at radii $r_{500} < r < 10 \text{ deg}$. In this analysis RMs in the lines of sight to clusters were excluded.

Figure 3 shows the distribution of the RMs in sky regions surrounding the clusters as a function of the mean RM in each region containing these sight-lines. On average, 21 RMs are found in each of the outskirts regions. The figure shows that the RM scatter is quite large. It is in general larger than the mean

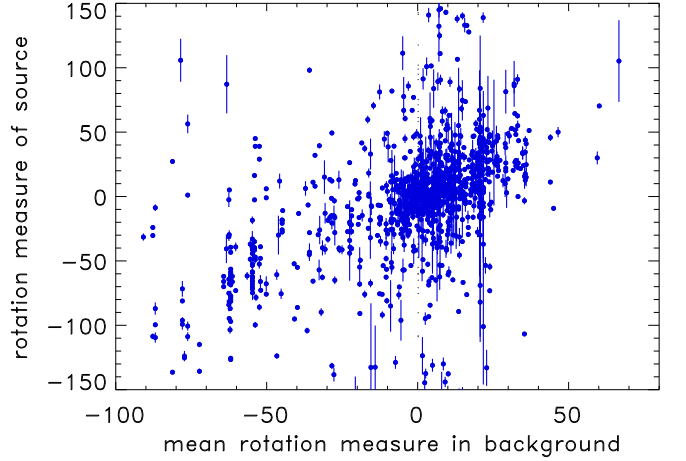


Fig. 3. Rotation measures in the outskirts of all clusters in our sample at a radius $> r_{500}$ and within 10 Mpc as a function of the mean rotation measure in each of the regions. Lines of sight falling into one of the clusters in our sample have been excised.

value we wish to use to correct for the Galactic RM contribution. However, the individual RMs are also clearly correlated with the mean. This clear correlation implies that we can improve on the measurement of the extragalactic RMs by subtracting the mean of the foreground RM that is detected in regions excluding clusters. To be conservative, we included the scatter in the determination of the average RM in the uncertainty of the corrected extragalactic RM.

This suggests a correction for the foreground emission measure by subtracting the mean of the foreground signal seen in the cluster outskirts from the observed cluster RM. The large RM scatter in each background area is then accounted for by including the scatter of the uncertainty of the corrected cluster RM.

Figure 4 shows the RMs corrected in this way as a function of the cluster-centric radius scaled to r_{500} . The signal barely changes in comparison to the uncorrected data shown in Fig. 1, as can also be seen in Table 1. We have also studied how the correction for Galactic contributions changes when we decrease the size of the background region around the cluster. Changing the outer radius of the background region between 5 and 10 deg causes differences in the results that are much smaller than the uncertainties.

To obtain more quantitative results as a function of the physical properties of the cluster ICM, we determined the electron column density of the ICM in the line of sight of the radio sources and inspected the RMs as a function of the electron column density according to Eq. 1. To model the ICM density distribution of the clusters, we assumed that the clusters are spherically symmetric and can be described by a self-similar model, scaling with the cluster mass or X-ray luminosity. We based the model on the results of our study of the REXCESS sample (Böhringer et al. 2007, Croston et al. 2008). We used the following parameterised function, which describes the electron density profile well:

$$n_e(r) = A \left(\frac{r}{r_c} \right)^\alpha \left[1 + \left(\frac{r}{r_c} \right)^2 \right]^{-\frac{3\beta}{2} + \frac{\alpha}{2}}. \quad (4)$$

This functional form was now fitted to the electron density profiles of the REXCESS sample clusters by scaling the radii to

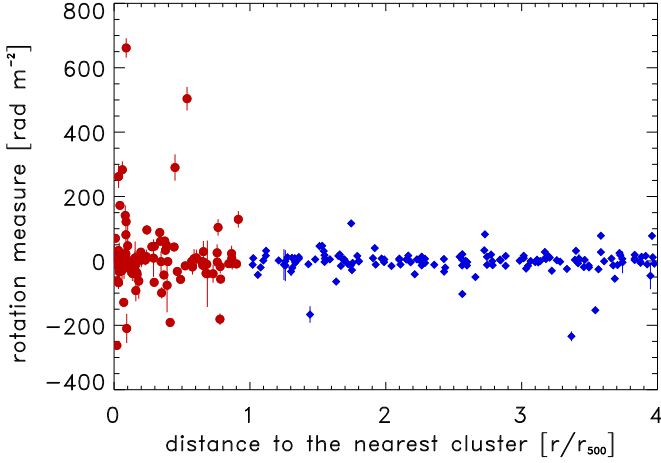


Fig. 4. Corrected rotation measures as a function of cluster-centric radius scaled by r_{500} .

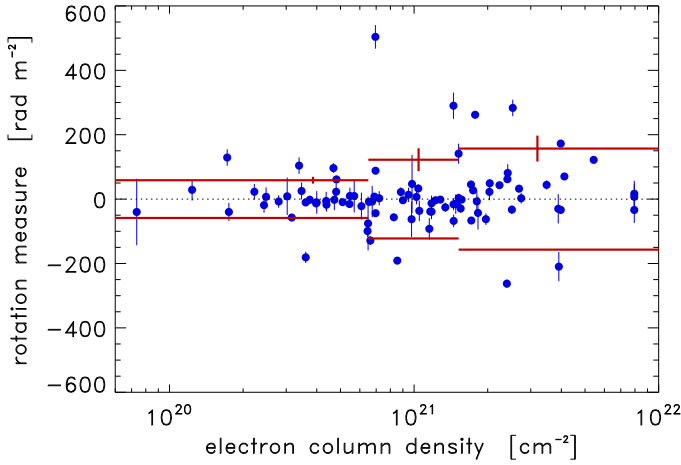


Fig. 5. Rotation measure as a function of electron column density of the ICM in the sight-line. The red bars give the dispersion of the rotation measures in three bins with error bars shown only on the positive side.

r_{500} and applying self-similar scaling. The resulting best-fitting parameters are $\alpha = 0.41$ and $\beta = 0.64$. The normalisation of the function is consistent with a gas mass fraction of the clusters of about 10%. For each line of sight we integrated the electron density out to r_{500} . Since several radio sources sit inside clusters, we integrated the column densities for these systems only over the half sphere, whereas we used the full sphere for the rest, including the radio sources without known redshifts.

Figure 5 shows the results of the corrected RMs as a function of estimated electron column density. In addition, the plot shows the RM scatter in three bins of the column density, with values of 58.6 ± 10.5 , 122.3 ± 35.6 , and 157.0 ± 40.3 rad m^{-2} . Again the RMs clearly increase with electron column density in the line of sight. The uncertainties for the scatter were obtained with 1000 bootstrap simulations in each case. The scatter in the lowest bin of the electron column density is almost identical to that in the surroundings of the clusters. This is not surprising given the low electron column densities in this bin, which can be taken as a baseline for the effect of the Galactic foreground. We subtracted it from the observed values in the other two bins in quadrature.

These results permit us to estimate the magnetic field by means of Eq. 1. Defining the electron column density $N_e = n_e \times L$ and assuming in a first step that the magnetic field is ordered on cluster scale, we obtain

$$\left(\frac{B_{\parallel}}{1\mu\text{G}}\right) = 3.801 \times 10^{18} \left(\frac{RM}{\text{rad m}^{-2}}\right) \left(\frac{N_e}{\text{cm}^{-2}}\right)^{-1} \quad (5)$$

Now we have to consider that the observed RM originates in the superposition of many ICM plasma cells in the line of sight with different magnetic field orientations. The RM will thus be diluted by averaging over all cells in the line of sight by a factor of $\Lambda = (L/l)^{1/2}$, where L is the length of the ICM column and l is the typical size of the plasma cells with coherent magnetic field direction. We can then calculate the line of sight magnetic field strength as

$$\left(\frac{B_{\parallel}}{1\mu\text{G}}\right) = 3.801 \times 10^{18} \left(\frac{\sigma(RM)}{\text{rad m}^{-2}}\right) \left(\frac{N_e}{\text{cm}^{-2}}\right)^{-1} \Lambda \quad (6)$$

where N_e in the electron column density in the line of sight. With values for the mean N_e in the second and third bin in Fig. 5 (1.04×10^{21} and 3.19×10^{21} cm^{-2}) and assuming typical values of $L \sim 1$ Mpc and $l \sim 10$ kpc, we find for the line of sight magnetic field component values of $0.38 (\pm 0.13) \times \Lambda$ and $0.17 (\pm 0.04) \times \Lambda$ μG . Combining the two bins yields a value of $0.18 (\pm 0.05) \times \Lambda$ μG . Typical coherence lengths of the magnetic field have been found to be in the range 2 - 25 kpc (e.g. Feretti et al. 1999, Govoni et al., 2001, Taylor et al. 2001, Eilek & Owen 2002, Murgia et al. 2004). This is interestingly similar to the value measured by Kim et al. (1990) from the projected RM variation along the cluster-internal extended radio source 5C4.81. Consequently, we scaled our results to $l = 10$ kpc. Assuming that the magnetic field is isotropic globally, an average column length of 1 Mpc, and a cell size of about 10 kpc, we find a total magnetic field a value of $\langle |B| \rangle \sim 3 \left(\frac{+3}{-1}\right) \times (l/10\text{kpc})^{-1/2}$ μG . This value confirms our previous results reported in Clarke et al. (2001) and agrees well in general with values quoted in the literature for the magnetic fields on global scales from equipartition considerations of radio halos and Faraday rotation measurements (e.g. Feretti et al. 2012).

We can further refine our model by allowing the magnetic field to vary within the cluster. A reasonable assumption is that the magnetic energy density has a constant ratio to the thermal energy density (e.g. Miniati 2015 and Miniati & Beresnyak 2015). This results from a dynamo action model, which amplifies the magnetic field in a turbulent ICM and saturates when the magnetic energy density reaches a certain fraction of the thermal energy density. This is typically of a few percent.

Thus we assume that

$$\frac{B^2}{8\pi} = \eta \frac{3}{2} n k_B T \quad (7)$$

where η gives the energy density ratio between the magnetic field and the thermal ICM. We also assume for simplicity that the cluster is isothermal. The RM scatter can then be predicted from the electron density distribution, the cluster temperature, and the parameter η ,

$$\begin{aligned} \sigma(RM) &\propto \eta^{1/2} \Lambda^{-1} 3^{-1/2} T^{1/2} \int n_e^{1.5} dl \\ \sigma(RM) &\propto \tilde{\eta}^{1/2} T^{1/2} \int n_e^{1.5} dl \quad (8) \end{aligned}$$

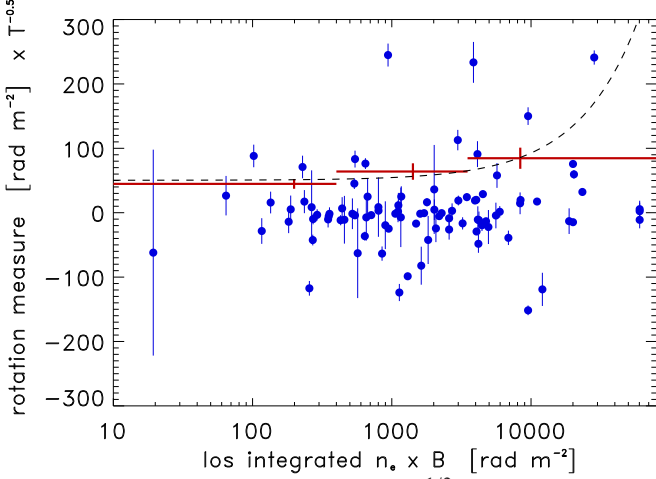


Fig. 6. Rotation measure scaled by $T^{1/2}$ as a function of the line of sight integrated electron density \times magnetic field strength. The red bars show the scatter of the scaled rotation measure in three bins with uncertainties. The dashed line shows the best fit to the scatter of the rotation measure.

with a factor of $3^{1/2}$ entering, because we consider the total magnetic field energy density, but only the line of sight component affects the RM.

By comparing a scaled RM to the predicted RM, we can obtain the unknown ratio parameter η . In Fig. 6 we plot $\frac{RM}{T^{1/2}}$ versus the predicted RM assuming $\eta = 1$ for the value given on the x-axis. The slope of this plot reflects $\tilde{\eta}^{1/2}$, which is about 0.004 – 0.005, shown as a dashed line in the plot. Adopting the parameter $\Lambda \sim 10$ and all three spatial components of the magnetic field for a globally isotropic configuration, this yields a value for η of $5 - 7.5 \times 10^{-3}$. Including additional uncertainties, we obtain an estimate of the ratio of magnetic to thermal energy density of $3 - 10 \times 10^{-3} (l/10kpc)^{-1/2}$.

5. Summary and conclusion

Comparing Faraday RMs of polarised extragalactic radio sources in the line of sight of galaxy clusters with RM measurements made outside the projected cluster regions, we find a clear excess of the standard deviation of the RM values in the cluster areas. The number of RM measurements is a factor of four larger than that in our previous study reported by Clarke et al. (2001). From the values given in Table 1, we deduce a significance of the signal above the background of $7 - 8\sigma$, as determined in the studies labelled A and C in the table.

Given these improved statistics, we can now better correlate RM measurements with physical parameters of the clusters. We find that the scatter in the RM values clearly increases with cluster mass and electron column density in the line of sight as estimated for our fiducial cluster model. From the correlation of the RM scatter with electron column density, we deduce a typical magnetic field strength of $2 - 6 (l/10kpc)^{-1/2} \mu\text{G}$, with the implicit assumption that the magnetic field is constant throughout the cluster. This result implies that the energy density in the magnetic field and its pressure is typically a few percent of the thermal energy density. In an alternative model for the ICM magnetic field in which we assumed that the magnetic field energy density is proportional to the thermal energy density, we found that the energy in the magnetic field is only several per mille of the thermal energy. The difference in the two results shows

that the outcome of the modelling depends on the way physical quantities are averaged over the cluster volume. For a magnetic field that correlates with the ICM energy density or pressure, the RM effect depends with a higher power than linearity on the density, the central region has a larger effect, and the overall energy required for the magnetic field is lower. A similar result has been found in the study of Murgia et al. (2004), where the magnetic field energy was modelled by a power spectrum. The required magnetic field strength for the detailed model was lower than that for the assumption of a homogeneous magnetic field. Therefore we conclude that from averaging over the entire cluster volume (out to r_{500}), the magnetic field energy is slightly lower than 1% of the thermal energy.

This has important implications for cluster mass measurements based on the hydrostatic equilibrium of the ICM plasma, where neglecting the magnetic field pressure would lead to an underestimate of the cluster mass. For total mass estimates out to a radius of r_{500} , for example, the magnetic field at larger cluster radii matters, and according to the above discussion, we expect the magnetic field there to contribute less than about 1% to the ICM pressure, making it a negligible effect in the error budget of current cluster mass measurements.

Finally, and in this context, it is interesting to compare clusters with the interstellar medium of our Galaxy. While for our Galaxy we typically find that the energy density in the magnetic field and in cosmic rays is comparable to the thermal energy density (Jenkins & Tripp 2011, Draine 2011), where the magnetic field in the Milky Way disk is about $0.6 \mu\text{G}$ (e.g. Heiles & Crutcher 2005, Kronberg 2016), and the magneto-ionic thickness has been estimated between 1 and 1.8 kpc (Simard-Normandin & Kronberg 1980, Sun et al., 2008, Gaensler et al. 2008). In contrast, galaxy clusters appear to have a lower ratio of $\varepsilon(B)/\varepsilon$ (thermal).

What makes these ratios different? In clusters the driving force of the energetic processes is gravitation in the merging of subunits to form a cluster. This is also the main energy source to generate turbulence and a magnetic field.¹ In the Galaxy the energy input into the ICM and cosmic rays comes mostly from supernovae and to some degree also indirectly from the differential rotation of the galaxy system. Even though the two systems seem to have many properties in common, the main energy source is therefore very different. For clusters the formation process and the generation of a cluster-wide magnetic field has been simulated in detailed magneto-hydrodynamic simulations in a cosmological model frame (e.g. Miniati 2014), and it was concluded that the dynamo action in a turbulent ICM can generate a magnetic field of the strength that is observed. The magnetic field amplification saturates, however, when the magnetic field energy density reaches about 2 - 3 percent of the thermal energy density (Beresnyak 2012, Miniati & Beresnyak 2015). The way in which the magnetic field is generated during the formation of the clusters therefore provides a natural way to set an upper limit on the possible magnetic field energy density. The generation of the magnetic field in our galaxy, which may be powered to a large extent by supernovae, is not subject to this upper limit.

Acknowledgements. H.B. and G.C. acknowledge support from the DFG Transregio Program TR33 and the Munich Excellence Cluster "Structure and

¹ Supermassive black holes in the central dominant galaxy can also contribute to the generation of turbulence in clusters. For very massive clusters this will mostly affect the central region, however. The RM signal that we detect comes mostly from massive clusters and is detected globally. In this case, we expect that the influence of supermassive black holes is rather limited.

Evolution of the Universe". G.C. acknowledges support from the DLR under grant no. 50 OR 1403, and P.P.K. thanks the Natural Sciences and Engineering Research Council of Canada for support under Discovery Grant No. A5713. H.B. and G.C. thank the University of Toronto for support during the visit. H.B. thanks Joachim Trümper for stimulating discussions.

References

- Böhringer, H., Voges, W., Huchra, J.P., et al., 2000, *ApJS*, 129, 435
 Böhringer, H., Schuecker, P., Guzzo, L., et al., 2004, *A&A*, 425, 367
 Böhringer, H., Schuecker, P., Pratt, G.W., et al., 2007, *A&A* 469 363
 Böhringer, H., Werner, N., 2010, *A&ARv*, 18, 127
 Böhringer, H., Chon, G., Collins, C.A., et al., 2013, *A&A*, 555, A30
 Carilli, C.L. & Taylor, G.B., 2002, *ARA&A*, 40, 319
 Chon, G., & Böhringer, H., 2012, *A&A*, 538, 35
 Chon, G., Böhringer, H., Smith, G.P., 2012, *A&A*, 548, A59
 Clarke, T.E., Kronberg, P.P., Böhringer, H., 2001, *ApJ*, 547, L111
 Croston, J.H., Pratt, G.W., Böhringer, H., et al., 2008, *A&A*, 487, 431
 Dickey, J.M., Lockman, F.J., 1990, *ARA&A*, 28, 215
 Draine, B., 2011, *Physics of the interstellar and intergalactic medium*, Princeton Univ. Press
 Eilek, J.A. & Owen, F.N., 2002, *ApJ*, 567, 202
 Feretti, L., Dallacasa, D., Giovannini, G., et al., 1995, *A&A*, 302, 680
 Feretti, L., Dallacasa, D., Govoni, F., et al., 1999, *A&A*, 344, 472
 Feretti, L., Giovannini, G., Govoni, F., et al., 2012, *A&ARv*, 20, 54
 Gaensler, B.M., Madsen, G.J., Chatterjee, S., & Mao, S.A., 2008, *Publ. Astron. Soc. of Australia*, 25, 184
 Govoni, F., Taylor, G.B., Dallacasa, D., et al., 2001, *A&A*, 379, 807
 Heiles, C. & Crutcher, R., 2005, in *Cosmic Magnetic Fields*, R. Wielebinski, R. Beck (eds.), *Lecture Notes in Physics*, 664, 137
 Jenkins, E.B., Tripp, T.M., 2011, *ApJ*, 734, 65
 Kim, K.-T., Kronberg, P.P., Dewdney, P.E., 1990, *ApJ*, 355, 29
 Kim, K.-T., Tribble, P.C., Kronberg, P.P., 1991, *ApJ*, 379, 80
 Kravtsov, A.V. & Borgani, S., 2012, *ARA&A*, 50, 353
 Kronberg, P.P. & Newton-McGee, K.J., 2011, *Publ. Astron. Soc. of Australia*, 28, 171
 Kronberg, P.P., Kothes, R., Salter, C.J., Perilat, P., 2007, *ApJ*, 659, 267
 Kronberg, P.P., 2016, *Cosmic Magnetic Fields*, Cambridge University Press, (in press)
 Lawler, J.M. & Dennison, B., 1982, *ApJ*, 252, 81
 Miniati, F., & Beresnyak, A., 2015, *Nat.*, 523, 59
 Miniati, F., 2015, *ApJ*, 800, 60
 Murgia, M., Govoni, F., Feretti, L., et al., 2004, *A&A*, 424, 429
 Owen, F.N. & Ledlow, M.J., 1997, *ApJS*, 108, 41
 Pshirkov, M.S., Tinyakov, P.G., Kronberg, P.P., & Newton-McGee, K.J., 2011, *ApJ*, 738, 192
 Simard-Normandin, M. & Kronberg, P.P., 1980, *ApJ*, 242, 74
 Simard-Normandin, M., Kronberg, P.P., Button, S., 1981, *ApJS*, 45, 97
 Sun, X.H., Reich, W., Waelkens, A., & Ensslin, T.E., *A&A* 477, 573
 Taylor, A.R., Stil, J.M., Sunstrum, C., 2009, *ApJ*, 702, 1230
 Taylor, G.B., Govoni, F., Allen, S.W., et al., 2001, *MNRAS*, 326, 2
 Trümper, J., 1993, *Science*, 260, 1769
 Voges, W., Aschenbach, B., Boller, T., et al. 1999, *A&A*, 349, 389
 Voit, M.G., 2005, *RvMP*, 77, 207
 Xu, Y., Kronberg, P.P., Habib, S., et al., 2006, *ApJ*, 637, 19